

Curvature of the chiral pseudo-critical line in QCD: continuum extrapolated results

Claudio Bonati,^{*} Massimo D'Elia,[†] Marco Mariti,[‡] Michele Mesiti,[§] and Francesco Negro[¶]
Dipartimento di Fisica dell'Università di Pisa and INFN - Sezione di Pisa,
Largo Pontecorvo 3, I-56127 Pisa, Italy

Francesco Sanfilippo^{**}
School of Physics and Astronomy, University of Southampton, SO17 1BJ Southampton, United Kingdom
 (Dated: September 1, 2015)

We determine the curvature of the pseudo-critical line of strong interactions by means of numerical simulations at imaginary chemical potentials. We consider $N_f = 2 + 1$ stout improved staggered fermions with physical quark masses and the tree level Symanzik gauge action, and explore four different sets of lattice spacings, corresponding to $N_t = 6, 8, 10, 12$, in order to extrapolate results to the continuum limit. Our final estimate is $\kappa = 0.0135(20)$.

PACS numbers: 12.38.Aw, 11.15.Ha, 12.38.Gc, 12.38.Mh

I. INTRODUCTION

The exploration of the phase diagram of strongly interacting matter in the temperature - baryon chemical potential ($T - \mu_B$) plane is being pursued both by experimental and by theoretical investigations. The comparison between the chemical freeze-out line [1–8] and the crossover line, corresponding to chiral symmetry restoration, is one of the main issues. In principle these two lines are not expected to coincide, however an exact statement about their interrelation will provide useful information about the dynamics of strong interactions. That requires a precise determination of both lines.

From the theoretical point of view, Lattice QCD simulations represent the best first principle tool to provide information about the chiral transition¹ temperature T_c : present results provide consistent evidence for $T_c \simeq 155$ MeV at $\mu_B = 0$. Unfortunately, as one moves to finite baryon chemical potential, direct numerical simulations are presently hindered by the so-called sign problem, stemming from the complex nature of the fermion determinant when $\mu_B \neq 0$. However, various methods have been proposed to circumvent the problem in the regime of small chemical potentials, where the pseudo-critical line can be well approximated by a quadratic behavior²

in μ_B^2 :

$$\frac{T_c(\mu_B)}{T_c} = 1 - \kappa \left(\frac{\mu_B}{T_c} \right)^2 + O(\mu_B^4), \quad (1)$$

where the coefficient κ defines the curvature of the pseudo-critical line $T_c(\mu_B)$. Information about κ can be obtained for instance by Taylor expansion techniques [14–17]), by analytic continuation from imaginary chemical potentials [18–29], by reweighting techniques [30, 31] or by a reconstruction of the canonical partition function [32, 33].

Recent numerical investigations [28, 29], adopting the method of analytic continuation with improved discretizations at or close to the physical point of $N_f = 2 + 1$ QCD, have provided results for κ which are generally larger than previous estimates obtained by the Taylor expansion technique [15–17].

In particular, in Ref. [29] we performed numerical simulations adopting an improved stout staggered fermion discretization on lattices with $N_t = 6, 8$, leading to a preliminary estimate $\kappa \sim 0.013$, to be compared with previous determinations obtained by Taylor expansion [15–17], reporting $\kappa \sim 0.006$.

In the present study we aim at extending our results in two directions. First, we increase the number of imaginary chemical potentials explored on lattices with $N_t = 8$, in order to obtain a better control over the analytic continuation systematics and to perform a deeper comparison between the cases in which a strange quark chemical potential is included or not. Then we extend simulations for $\mu_s = 0$ to two new sets of lattice spacings, corresponding to $N_t = 10$ and $N_t = 12$, in order to perform a continuum extrapolation of our determination of κ . As a byproduct, we also discuss the behavior of the continuum extrapolated chiral susceptibilities as a function of μ_B , in order to assess the possible influence of the baryon chemical potential on the strength of the transition, which is relevant to the possible existence of a critical endpoint in the $T - \mu_B$ plane.

The paper is organized as follows. In Section II we provide some details about the lattice discretization adopted

^{*}Electronic address: bonati@df.unipi.it

[†]Electronic address: delia@df.unipi.it

[‡]Electronic address: mariti@df.unipi.it

[§]Electronic address: mesiti@pi.infn.it

[¶]Electronic address: fnegro@pi.infn.it

^{**}Electronic address: f.sanfilippo@soton.ac.uk

¹ We speak of chiral transition even if present lattice studies provide evidence for a crossover [9–13].

² We note that a possible ambiguity in the denominator of the quadratic term, i.e. whether we take $\mu_B/T_c(\mu_B)$ or $\mu_B/T_c(0)$ as an expansion variable, is irrelevant as long as just the quadratic term is considered, since it only affects higher order terms.

in this study, about the various explored setups of chemical potentials, about the observables chosen to locate T_c and their renormalization. In Section III we discuss our numerical results and finally, in Section IV, we draw our conclusions.

II. NUMERICAL SETUP

As in Ref. [29], we consider a lattice discretization of $N_f = 2 + 1$ QCD in the presence of purely imaginary quark chemical potentials. We consider the following euclidean partition function

$$\mathcal{Z} = \int \mathcal{D}U e^{-\mathcal{S}_{YM}} \prod_{f=u,d,s} \det \left(M_{\text{st}}^f[U, \mu_{f,I}] \right)^{1/4}, \quad (2)$$

$$\mathcal{S}_{YM} = -\frac{\beta}{3} \sum_{i,\mu \neq \nu} \left(\frac{5}{6} W_{i;\mu\nu}^{1 \times 1} - \frac{1}{12} W_{i;\mu\nu}^{1 \times 2} \right), \quad (3)$$

$$\begin{aligned} (M_{\text{st}}^f)_{i,j} &= am_f \delta_{i,j} + \sum_{\nu=1}^4 \frac{\eta_{i;\nu}}{2} \left[e^{ia\mu_{f,I}\delta_{\nu,4}} U_{i;\nu}^{(2)} \delta_{i,j-\hat{\nu}} \right. \\ &\quad \left. - e^{-ia\mu_{f,I}\delta_{\nu,4}} U_{i-\hat{\nu};\nu}^{(2)\dagger} \delta_{i,j+\hat{\nu}} \right]. \end{aligned} \quad (4)$$

where U are the gauge link variables, \mathcal{S}_{YM} is the tree level improved Symanzik gauge action [34, 35], written in terms of $W_{i;\mu\nu}^{n \times m}$ (trace of the $n \times m$ loop constructed from the gauge links along the directions μ, ν departing from the i site). Finally, the staggered Dirac operator $(M_{\text{st}}^f)_{i,j}$ is built up in terms of the two times stout-smearing [36] links $U_{i;\nu}^{(2)}$, with an isotropic smearing parameter $\rho = 0.15$. Stout smearing improvement is used in order to reduce taste symmetry violations (see Ref. [37] for a comparison among different improved staggered discretizations); the rooting procedure is exploited, as usual, to remove the residual fourth degeneracy of the staggered lattice Dirac operator (see, e.g., Ref. [38] for a discussion on possible related systematics).

The temperature of the system is given by $T = 1/(N_t a)$, where a is the lattice spacings and N_t is the number of lattice sites in the temporal direction, along which we take thermal boundary conditions (periodic/antiperiodic for boson/fermion fields). At fixed N_t , T is changed by varying the value of the bare coupling constant β . The bare quark masses m_s and m_l are rescaled accordingly, in order to move on a line of constant physics, with $m_\pi \simeq 135$ MeV and $m_s/m_l = 28.15$. This line is determined by a spline interpolation of the values reported in Refs. [39, 40] (see also Ref. [29]). Four different sets of lattice spacings, corresponding to $N_t = 6, 8, 10, 12$, have been explored, in order to extrapolate our results to the continuum limit.

A. Setup of chemical potentials

In Eq. (2), we have introduced an imaginary chemical potential $\mu_f = i\mu_{f,I}$, $\mu_{f,I} \in \mathbb{R}$, with $f = u, d, s$, coupled to the number operator of each quark flavor. They are related to the chemical potentials coupled to conserved charges (baryon number B , electric charge Q and strangeness S) by the following relations

$$\begin{aligned} \mu_u &= \mu_B/3 + 2\mu_Q/3 \\ \mu_d &= \mu_B/3 - \mu_Q/3 \\ \mu_s &= \mu_B/3 - \mu_Q/3 - \mu_S. \end{aligned} \quad (5)$$

The purpose of our study is to determine the dependence of the pseudocritical temperature T_c on the baryon chemical potential (which is given by $\mu_B = \mu_u + 2\mu_d$), in a setup of chemical potentials which is as close as possible to the thermal equilibrium conditions created in heavy ion collisions. We thus have to require to $S = 0$ and $Q = rB$, where r is the number of protons divided by the number of nucleons of the colliding ions, $r \equiv Z/A \approx 0.4$ typically.

These requirements can be translated into relations between μ_B , μ_S and μ_Q , which at the lowest order in μ_B read $\mu_Q \simeq q_1(T)\mu_B$ and $\mu_S \simeq s_1(T)\mu_B$, the coefficients $q_1(T)$ and $s_1(T)$ being related to derivatives of the free energy density [41, 42]. Let us consider as an example the strangeness neutrality condition: in a gas of non-interacting fermions it would imply $\mu_s = 0$ but in QCD, due to interactions, the mixed derivatives of the free energy density with respect to μ_s and μ_u, μ_d are non-vanishing, so that one needs a non-zero μ_s to ensure $S = 0$. Present lattice investigations [41, 42] show that, for $T \sim 155$ MeV, the constraints on charge and strangeness imply $s_1 \simeq 0.25$ and $q_1 \simeq -0.025$. With a precision of a few percent, around the transition at vanishing density, we thus have $\mu_l \equiv \mu_u = \mu_d$, $\mu_l \simeq \mu_B/3$ and $\mu_s \simeq \mu_l/4$.

Our determination of the curvature κ has been obtained setting $\mu_s = 0$, which is close to the conditions described above. To quantify the impact of μ_s , as in Ref. [29], we have considered also the case $\mu_s = \mu_l$, in order to obtain an estimate about the effect of a non-zero μ_s in a range which covers the equilibrium conditions created in heavy ion collisions.

B. Physical observables, renormalization and the determination of T_c

In the absence of a true phase transition, the determination of the pseudo-critical line may depend on the physical observable chosen to locate it. On the other hand, chiral symmetry restoration is the leading phenomenon around T_c , with the light chiral condensate becoming an exact order parameter in limit of zero light quark masses. Therefore in the following $T_c(\mu_B)$ will be determined by monitoring the chiral properties of the

system. The chiral condensate of the flavor f is defined as

$$\langle \bar{\psi}\psi \rangle_f = \frac{T}{V} \frac{\partial \log Z}{\partial m_f}, \quad (6)$$

where V is the spatial volume. In our simulations the two light quarks are degenerate, $m_l \equiv m_u = m_d$, and it is convenient to introduce the light quark condensate:

$$\langle \bar{\psi}\psi \rangle_l = \frac{T}{V} \frac{\partial \log Z}{\partial m_l} = \langle \bar{u}u \rangle + \langle \bar{d}d \rangle; \quad (7)$$

$\langle \bar{\psi}\psi \rangle_l$ is affected by both additive and multiplicative renormalizations. We consider two different renormalization prescriptions, in order to determine whether any systematic effect related to this choice affects the determination of κ . The first one [43] is

$$\langle \bar{\psi}\psi \rangle_{(1)}^r(T) \equiv \frac{\left[\langle \bar{\psi}\psi \rangle_l - \frac{2m_l}{m_s} \langle \bar{s}s \rangle \right](T)}{\left[\langle \bar{\psi}\psi \rangle_l - \frac{2m_l}{m_s} \langle \bar{s}s \rangle \right](T=0)}, \quad (8)$$

where m_s is the bare strange quark mass; in this way the leading mass dependent contribution is subtracted³, while one takes care of the multiplicative renormalization by dividing by the same quantity at $T = 0$. As an alternative, we consider the following prescription [16]

$$\langle \bar{\psi}\psi \rangle_{(2)}^r = \frac{m_l}{m_\pi^4} (\langle \bar{\psi}\psi \rangle_l - \langle \bar{\psi}\psi \rangle_l(T=0)). \quad (9)$$

In this case the zero T subtraction eliminates additive divergences while multiplication by the bare quark mass m_l takes care of multiplicative ones.

The behavior of both condensates will be monitored to locate T_c . In particular, since in the presence of a true phase transition the slope of the condensate as a function of T diverges at T_c , we will look for the point of maximum slope, i.e. the inflection point (a detailed comparison with other prescriptions has been reported in Ref. [29]).

A much better probe is provided by the chiral susceptibility $\chi_{\bar{\psi}\psi}$, which is itself divergent at T_c in the presence of a true transition: in this case the introduction of relevant parameters (finite mass or finite volume) smooths the divergence, however looking for the maximum of $\chi_{\bar{\psi}\psi}$ remains a well defined and univocal prescription for locating the pseudo-critical temperature T_c . On the lattice, the light chiral susceptibility is given by (M_l is the Dirac

operator corresponding to a single light flavor)

$$\chi_{\bar{\psi}\psi} = \frac{\partial \langle \bar{\psi}\psi \rangle_l}{\partial m_l} = \chi_{\bar{\psi}\psi}^{disc} + \chi_{\bar{\psi}\psi}^{conn} \quad (10)$$

$$\chi_{\bar{\psi}\psi}^{disc} \equiv \frac{T}{V} \left(\frac{N_l}{4} \right)^2 [(\text{Tr} M_l^{-1})^2] - \langle \text{Tr} M_l^{-1} \rangle^2 \quad (11)$$

$$\chi_{\bar{\psi}\psi}^{conn} \equiv -\frac{T}{V} \frac{N_l}{4} \langle \text{Tr} M_l^{-2} \rangle. \quad (12)$$

where $N_l = 2$ is the number of degenerate light quarks. The renormalization is performed by first subtracting the $T = 0$ contribution, to remove the additive renormalization, then multiplying the result by the square of the bare light quark mass, to cancel the multiplicative one [39]:

$$\chi_{\bar{\psi}\psi}^r = m_l^2 [\chi_{\bar{\psi}\psi}(T) - \chi_{\bar{\psi}\psi}(T=0)]. \quad (13)$$

C. Analytic continuation from imaginary chemical potentials

The physical observables relevant to our study will be monitored as a function of T for fixed values of the dimensionless ratio $\theta_l = \text{Im}(\mu_l)/T$. In this way we shall be able to locate T_c for a set of values of θ_l , so as to determine the dependence $T_c(\theta_l)$ to the leading order

$$\frac{T_c(\theta_l)}{T_c(0)} = 1 + R\theta_l^2 + O(\theta_l^4), \quad (14)$$

where we have assumed $T_c(\theta_l)$ to be an analytic function of θ_l , at least for small values of it. This assumption is consistent with numerical data and is at the basis of the method of analytic continuation. Comparing with Eq. (1) one has, at the leading order in μ_B^2 , $\kappa = R/9$.

III. NUMERICAL RESULTS

We have performed simulations on lattices with $N_t = 8, 10$ and 12 and different choices of T and of the chemical potentials; results will be combined with those already presented in Ref. [29] for $N_t = 6, 8$ to perform the continuum extrapolation. To that purpose, we will consider only lattices with fixed aspect ratio $L_s/N_t = 4$: that guarantees the absence of significant finite size effects (see Ref. [29] for a detailed study about that).

Four different values of chemical potentials have been considered for $N_t = 10, 12$, corresponding to $\mu_s = 0$ and $\text{Im}(\mu_l)/(\pi T) = 0, 0.20, 0.24$ and 0.275 . A larger set has been considered for $N_t = 8$, in which case we performed simulations also at $\mu_s \neq 0$, in order to provide more information about systematics related to the choice of μ_s/μ_l and to the truncation of the Taylor expansion in Eq. (14).

For each setup of chemical potentials we have explored $\mathcal{O}(10)$ different temperatures around $T_c(\theta_l)$. The Rational Hybrid Monte-Carlo algorithm [45–47] has been used

³ This prescription subtracts both divergent and finite terms which are linear in the mass, thus permitting to isolate contributions to the quark condensate directly related to spontaneous chiral symmetry breaking. However, possible additive logarithmic divergences could still be present.

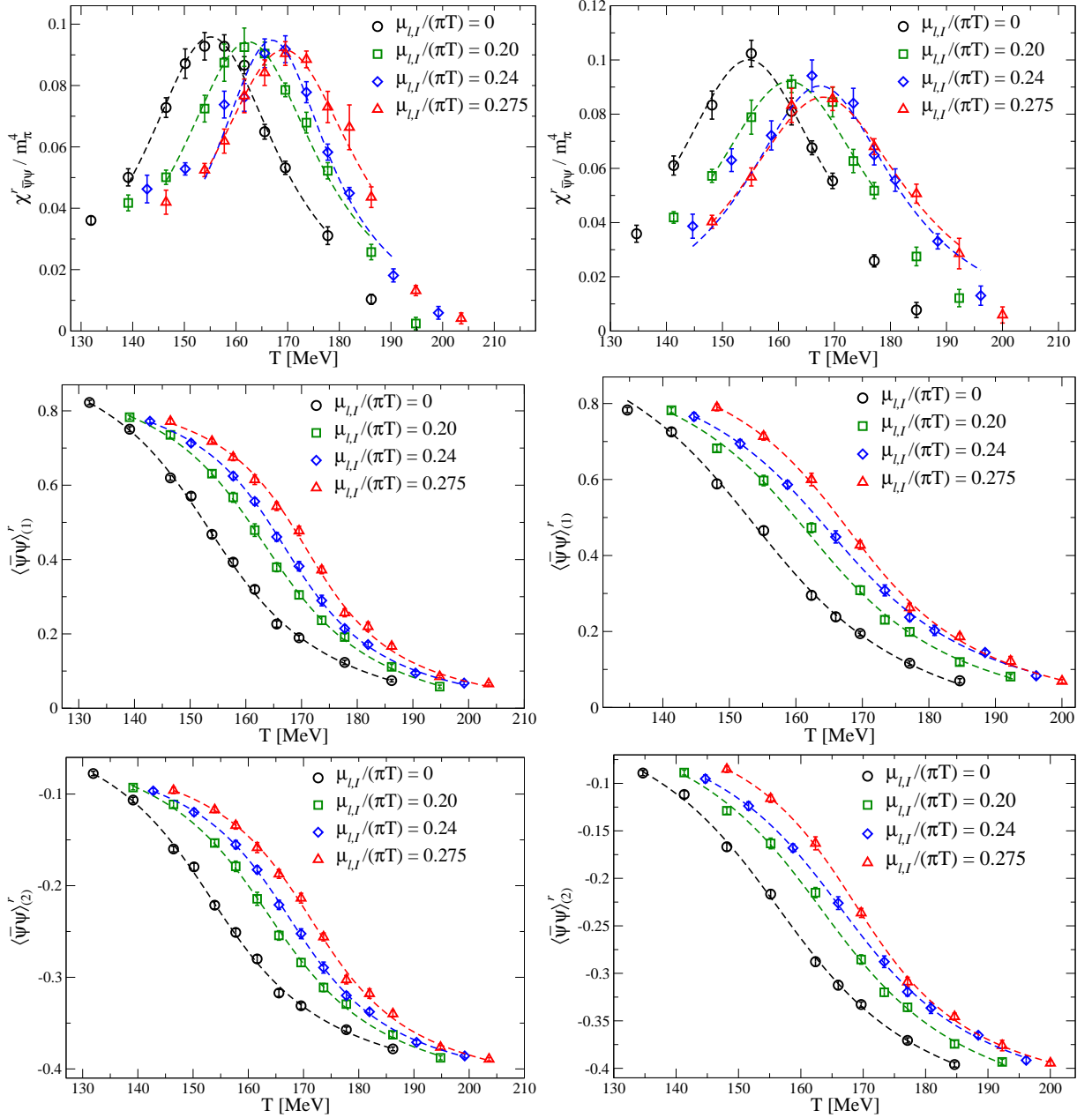


FIG. 1: Renormalized susceptibility and chiral condensates for the $40^3 \times 10$ (left column) and $48^3 \times 12$ lattices (right column).

to sample gauge configurations according to Eq. (2), each single run consisting of 2-5 K trajectories of unit length in molecular dynamics time, with higher statistics around the transition.

Traces appearing in the definition of chiral quantities (see, e.g., Eqs. (11) and (12)) have been computed by noisy estimators at the end of each molecular dynamics trajectory, using 8 random vectors for each flavor. Such a choice has appeared, after some preliminary tests, as a reasonable compromise to balance the effort spent in the stochastic estimators and in the gauge configuration production, i.e. in order to optimize the statistical error obtained for a given computational effort. A jackknife

analysis has been exploited to determine the statistical errors.

To perform the renormalization described in Sec. II, one needs to compute observables also at $T = 0$ and at the same values of the bare parameters, i.e. at the same ultraviolet (UV) cutoff. For that reason we have performed simulations on lattices as large as 48^4 : details are reported in Appendix A.

In order to determine the inflection point of the renormalized chiral condensate, we have performed a best fit to our data according to

$$\langle \bar{\psi} \psi \rangle^r(T) = A_1 + B_1 \arctan(C_1(T - T_c)) , \quad (15)$$

Lattice	$\frac{\mu_{LI}}{\pi T}$	$\frac{\mu_{sI}}{\pi T}$	$T_c(\bar{\psi}\psi_{(1)})$	$T_c(\bar{\psi}\psi_{(2)})$	$T_c(\chi^r)$
$16^3 \times 6$	0.00	0.00	148.2(3)	148.4(4)	150.7(4)
$16^3 \times 6$	0.20	0.00	155.0(4)	155.1(5)	157.0(4)
$16^3 \times 6$	0.24	0.00	158.9(4)	159.1(4)	160.0(4)
$16^3 \times 6$	0.275	0.00	161.2(4)	161.5(4)	162.7(4)
$24^3 \times 6$	0.00	0.00	149.0(6)	149.0(6)	151.6(5)
$24^3 \times 6$	0.24	0.00	160.8(7)	160.7(5)	162.0(5)
$24^3 \times 6$	0.275	0.00	164.1(4)	164.3(5)	165.9(4)
$32^3 \times 6$	0.00	0.00	149.1(7)	149.4(4)	152.0(4)
$32^3 \times 6$	0.24	0.00	160.2(3)	160.4(2)	162.7(4)
$32^3 \times 6$	0.275	0.00	163.4(3)	163.5(3)	165.5(4)
$32^3 \times 8$	0.00	0.00	154.2(4)	154.5(4)	155.6(7)
$32^3 \times 8$	0.10	0.00	155.4(7)	155.2(8)	157.2(7)
$32^3 \times 8$	0.15	0.00	159.5(9)	158.9(9)	160.2(5)
$32^3 \times 8$	0.20	0.00	162.9(8)	163.0(6)	163.0(6)
$32^3 \times 8$	0.24	0.00	165.0(5)	164.8(5)	165.8(8)
$32^3 \times 8$	0.275	0.00	169.5(9)	168.6(7)	169.8(7)
$32^3 \times 8$	0.30	0.00	172.4(9)	171.8(9)	172.8(8)
$32^3 \times 8$	0.10	0.10	157.1(8)	157.0(8)	158.5(7)
$32^3 \times 8$	0.15	0.15	159.2(9)	158.8(8)	160.1(8)
$32^3 \times 8$	0.20	0.20	163.9(6)	163.7(6)	165.3(9)
$32^3 \times 8$	0.24	0.24	169.4(7)	168.6(6)	169.6(7)
$32^3 \times 8$	0.275	0.275	175.4(6)	174.4(7)	177.0(8)
$40^3 \times 10$	0.00	0.00	154.5(1.5)	154.3(1.5)	155.1(7)
$40^3 \times 10$	0.20	0.00	163.0(7)	163.0(8)	162.5(7)
$40^3 \times 10$	0.24	0.00	166.8(8)	167.1(7)	166.2(1.0)
$40^3 \times 10$	0.275	0.00	170.8(8)	171.2(8)	169.6(8)
$48^3 \times 12$	0.00	0.00	154.5(1.0)	155.5(1.3)	154.7(7)
$48^3 \times 12$	0.20	0.00	163.2(1.2)	165.0(1.5)	161.9(7)
$48^3 \times 12$	0.24	0.00	165.2(1.1)	166.2(1.0)	166.2(1.0)
$48^3 \times 12$	0.275	0.00	167.8(1.2)	168.7(9)	167.9(9)

TABLE I: Critical values of T obtained from the renormalized chiral susceptibility and from the renormalized chiral condensates. Errors do not take into account the uncertainty on the physical scale, which is of the order of 2-3 % [39, 40].

which involves the independent parameters A_1 , B_1 , C_1 and T_c . Instead, for the determination of the peak of the renormalized susceptibility, we have performed a best fit according to a Lorentzian function

$$\chi_{\bar{\psi}\psi}^r = \frac{A_2}{B_2^2 + (T - T_c)^2}. \quad (16)$$

Both functions are found to well describe respective data points around T_c . In both cases, statistical errors on the fitted parameters have been estimated by means of a bootstrap analysis, while systematic uncertainties have been estimated either by varying the range of fitted points around T_c or by choosing an alternative fitting function (e.g., a hyperbolic tangent for the condensate or a parabola for its susceptibility). Statistical and systematic⁴ errors are both included in the collection of determinations of T_c for the various combinations of lattice

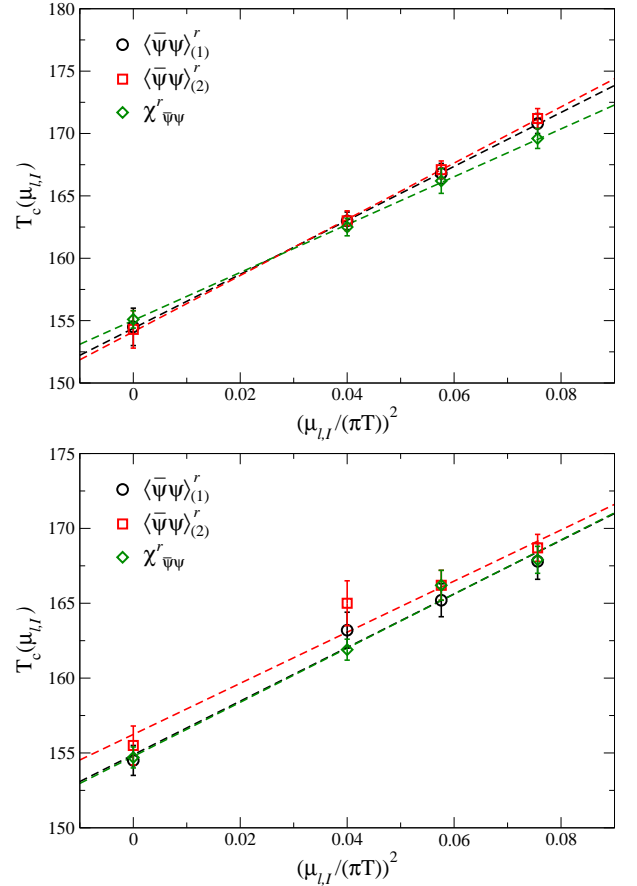


FIG. 2: Critical lines for the $40^3 \times 10$ lattice (top) and for the $48^3 \times 12$ one (bottom).

sizes and chemical potentials in Table I, which includes, for completeness, also results presented in Ref. [29].

In Fig. 1 we report results obtained for $\chi_{\bar{\psi}\psi}^r$, $\langle \bar{\psi}\psi \rangle_{(1)}^r$ and $\langle \bar{\psi}\psi \rangle_{(2)}^r$ on the $40^3 \times 10$ and $48^3 \times 12$ lattice, together with some best fits according to Eqs. (15) and (16). In the following we will perform the continuum limit using two different methods, in order to check for systematics effects.

Lattice	$\kappa(\bar{\psi}\psi_{(1)})$	$\kappa(\bar{\psi}\psi_{(2)})$	$\kappa(\chi^r)$
$24^3 \times 6$	0.0150(7)	0.00152(7)	0.0140(7)
$32^3 \times 8$	0.0142(7)	0.0135(7)	0.0134(9)
$40^3 \times 10$	0.0157(17)	0.0164(16)	0.0139(10)
$48^3 \times 12$	0.0130(15)	0.0123(17)	0.0131(11)

TABLE II: Curvatures obtained at fixed N_t from different observables.

physical scale, which is of the order of 2-3 % [39, 40] and, being related to an overall scale determination, does not affect the ratio of pseudocritical temperatures entering the determination of κ , see Eqs. (1) and (14).

⁴ We do not report the systematic error on the determination of the

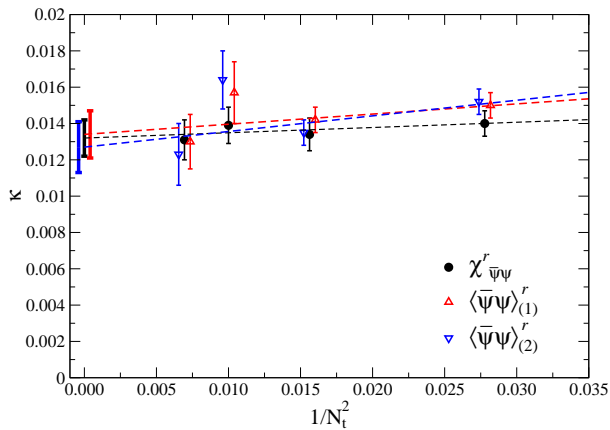


FIG. 3: Continuum limit of the curvatures extracted at fixed N_t (data have been slightly shifted in the horizontal direction to improve readability).

A. Continuum limit for $\mu_s = 0$ - First method

In order to extract the curvature of the critical line, we have performed a best fit to the values of $T_c(\mu_{l,I})$, obtained for each lattice size and setup of chemical potentials, according to the function

$$T_c(\mu_{l,I}) = T_c(0) \left(1 + 9\kappa \left(\frac{\mu_{l,I}}{T_c(\mu_{l,I})} \right)^2 + O(\mu_{l,I}^4) \right). \quad (17)$$

For all sets of chemical potentials explored for $\mu_s = 0$, the inclusion of quartic corrections has not been necessary: a more detailed discussion about the stability of the fit as the range of chemical potentials is changed is reported in Sec. III D.

In Fig. 2 we report an example of such quadratic fits to the critical temperatures obtained for $N_t = 10, 12$ and for the various explored observables. A complete collection of results, including also those already presented in Ref. [29], is reported in Table II.

In a range of temperatures around T_c , the UV cut-off a^{-1} is approximately proportional to N_t . Therefore, assuming corrections proportional to a^2 , we extracted, from the curvatures obtained for different values of N_t , continuum extrapolated results according to the ansatz

$$\kappa(N_t) = \kappa_{cont} + \text{const.}/N_t^2. \quad (18)$$

Results are shown in Fig. 3, where we also report the extrapolated continuum values, which are $\kappa_{cont}(\langle\bar{\psi}\psi\rangle_{(1)}^r) = 0.0134(13)$, $\kappa_{cont}(\langle\bar{\psi}\psi\rangle_{(2)}^r) = 0.0127(14)$ and $\kappa_{cont}(\chi_{\bar{\psi}\psi}^r) = 0.0132(10)$.

B. Continuum limit for $\mu_s = 0$ - Second method

Results of the previous section show that the continuum extrapolation of κ is quite smooth, with a good

agreement between the results obtained with different observables and different renormalization prescriptions. This is also consistent with the preliminary evidence reported in Ref. [29].

Nevertheless, it is useful to explore different ways of performing the continuum limit, in order to check for the overall consistency of the procedure. In the previous section we first determined the value of κ at each single value of N_t , then extrapolated these results to $N_t \rightarrow \infty$ to obtain κ_{cont} . A different procedure is to first extrapolate the critical temperatures to $N_t \rightarrow \infty$ (for fixed values of the dimensionless ratio $\mu_{l,I}/T$) and then to extract the value of κ_{cont} by using the continuum extrapolated critical temperatures.

To implement the second procedure we have performed, separately for each $\mu_{l,I}/T$, a best fit to the values obtained for the renormalized condensates and for the renormalized chiral susceptibility on different values of N_t , according to modified versions of Eqs. (15) and (16). Since the cut-off dependence is more pronounced for such quantities, we have excluded $N_t = 6$ data, thus using only $N_t = 8, 10, 12$.

In detail, in the case of the renormalized susceptibility, each fit parameter appearing in Eq. (16) has been given an additional N_t dependence, for instance $T_c(N_t) = T_c(N_t = \infty) + \text{const}/N_t^2$. Results for the extrapolated quantities are reported in the upper plot in Fig. 4 where, for the sake of clarity, we report only the cases $\mu_{l,I} = 0$ and $\mu_{l,I}/(\pi T) = 0.275$. In the case of the renormalized condensates, instead, due to the larger number of parameters which are present in Eq. (15), we could obtain fits which are stable against the variation of the fitted range by adding an N_t -dependence to just two parameters, in particular T_c and C_1 . Results are shown in the middle and lower plot of Fig. 4.

Such fits provide estimates for the continuum extrapolated pseudo-critical temperatures, reported in Table III and in Fig. 5. Such values coincide, within errors, with the continuum pseudo-critical temperatures that one could obtain by directly fitting results reported in Table I. A best fit to the extrapolated temperatures according to Eq. (17), with only the quadratic term included, provides $\kappa_{cont}(\langle\bar{\psi}\psi\rangle_{(1)}^r) = 0.0145(11)$, $\kappa_{cont}(\langle\bar{\psi}\psi\rangle_{(2)}^r) = 0.0138(10)$ and $\kappa_{cont}(\chi_{\bar{\psi}\psi}^r) = 0.0131(12)$, which are consistent with those found previously.

$\mu_{l,I}/(\pi T)$	$T_c(\psi\psi_{(1)})$	$T_c(\psi\psi_{(2)})$	$T_c(\chi^r)$
0.00	154.7(8)	156.5(8)	154.4(8)
0.20	163.9(8)	165.0(7)	161.0(1.1)
0.24	166.9(9)	168.5(7)	165.8(1.0)
0.275	169.7(8)	170.8(7)	167.3(1.1)

TABLE III: Continuum extrapolated critical temperatures for the various $\mu_{l,I}$ values.

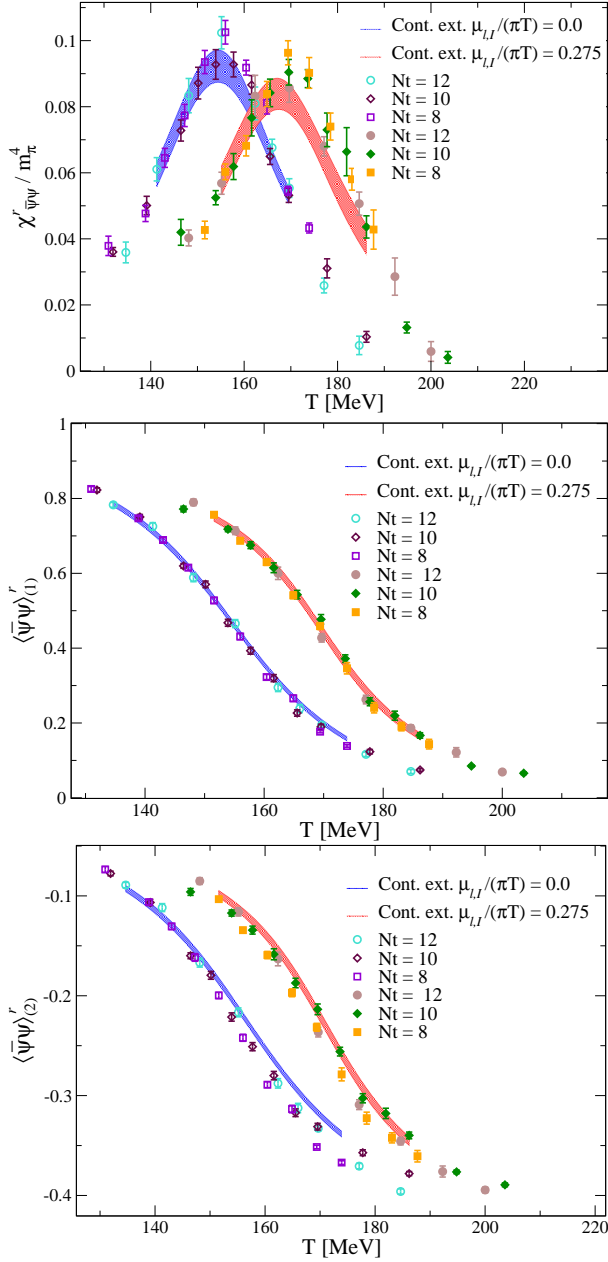


FIG. 4: Continuum limit for the renormalized susceptibility and the renormalized chiral condensates.

C. Strength of the transition as a function of μ_B

The width and the height of the chiral susceptibility peak, which can be obtained respectively from B_2 and A_2/B_2^2 in Eq. (16), are directly related to the strength of the chiral pseudo-transition. Therefore, we have the possibility to monitor the dependence of such strength on the baryon chemical potential and, having performed a continuum extrapolation for $\chi_{\bar{\psi}\psi}^r$, we can do that directly on continuum extrapolated quantities.

If a critical endpoint exists, along the pseudo-critical line, for relatively small values of real μ_B , we might ex-

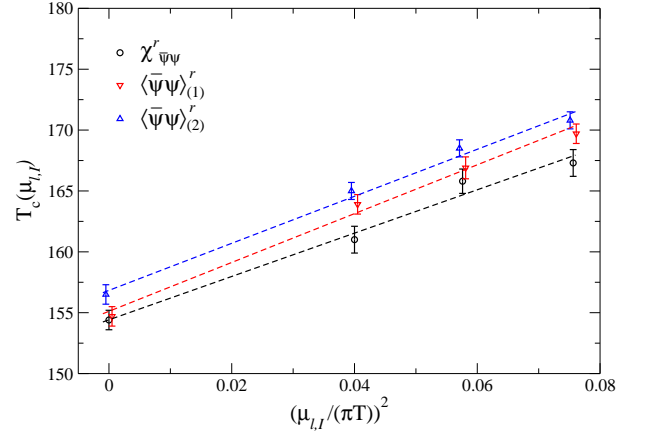


FIG. 5: Critical lines obtained by using the continuum extrapolated renormalized chiral susceptibility and the continuum extrapolated chiral condensates.

pect a visible dependence of the strength parameters also for small values of imaginary μ_B . The width and the height would tend respectively to zero and infinity approaching, e.g., a critical endpoint in the Z_2 universality class.

To that purpose, in Fig. 6 we plot the continuum extrapolated width B_2 and height A_2/B_2^2 as a function of $\mu_{l,I}$. No apparent change of either quantity can be appreciated, hence no dependence of the strength as a function of μ_B .

Of course, that does not exclude the presence of a critical endpoint at real μ_B : the critical region could be small enough, or the endpoint location far enough from $\mu_B = 0$, so that no influence is visible for small, imaginary μ_B . For instance, for $\mu_s = 0$, a Roberge-Weiss [44] like endpoint is expected along the pseudo-critical line at imaginary chemical potential, for $\mu_{l,I}/(\pi T) \sim 0.45$ [29]. Fig. 6 shows that also this endpoint has no apparent influence on the strength of the transition in the explored range.

D. Inclusion of $\mu_s \neq 0$ and systematics of analytic continuation

We have extended results for $N_t = 8$ presented in Ref. [29], performing numerical simulations for a larger range of imaginary chemical potentials, which include also the case $\mu_s = \mu_l$. That enable us to answer two important questions. What is the systematic error, in the determination of κ by analytic continuation, related to the truncation of the Taylor series in Eq. (17) and to the chosen range of chemical potentials? What is the impact of our effective ignorance about the actual value of μ_s corresponding to the thermal equilibrium conditions? We are going to discuss in detail only the determination of the pseudo-critical temperature from the renormalized chiral susceptibility, however we stress that similar

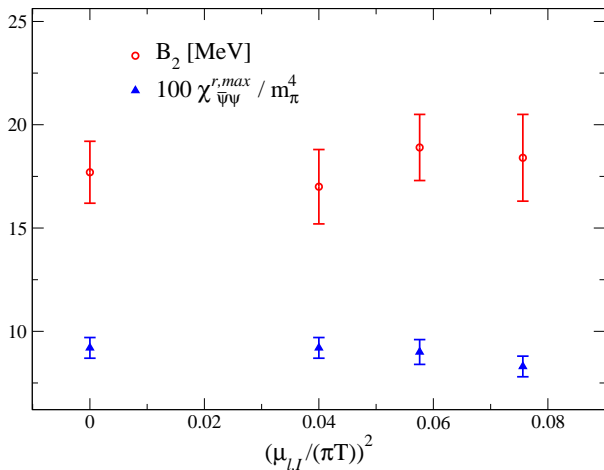


FIG. 6: Peak values ($\times 100$) and widths of the continuum extrapolated renormalized chiral susceptibility.

conclusions are reached when one considers the renormalized chiral condensate. The corresponding pseudo-critical temperatures, taken from Table I, are reported in Fig. 7 for $\mu_s = 0$ and for $\mu_s = \mu_l$.

We first tried a quadratic fit in $\mu_{l,I}$: remembering the definition $\theta_l = \mu_{l,I}/T$, we used

$$T_c(\theta_l) = T_c(0)(1 + 9\kappa\theta_l^2) \quad (19)$$

and several fits have been performed by changing each time the maximum value $\mu_{l,I}^{(max)}$ included in the fit. Reasonable best fits are obtained in all cases, apart from the fit to the whole $\mu_s = \mu_l$ range, which yields a reduced $\tilde{\chi}^2 \sim 2.4$ and indicates the need for quartic corrections in this case. Results obtained for κ are shown in Fig. 8: for $\mu_s = 0$, the fitted value of κ is perfectly stable as the range of chemical potentials is changed. Instead, for $\mu_s = \mu_l$, the value of κ clearly depends on the fitted range of chemical potentials: it is larger as the range is extended and becomes compatible, within errors, with that obtained for $\mu_s = 0$ as the range is decreased. This behavior is consistent with the presence of significant quartic corrections in this case. That may be related to the different structures of the phase diagrams for imaginary chemical potential that one has in the two cases: this issue has been discussed in detail in Ref. [29].

We then tried a best fit to a function including quartic corrections,

$$T_c(\theta_l) = T_c(0)(1 + 9\kappa\theta_l^2 + b\theta_l^4), \quad (20)$$

to the whole range of chemical potentials explored in both cases. The corresponding results obtained for κ are reported in Fig. 8 as well. While for $\mu_s = 0$ the value is perfectly compatible with the one obtained without including quartic corrections (indeed, in this case one obtains $b = 0$ within errors), for $\mu_s = \mu_l$ we observe a significant change, bringing κ in good agreement with the $\mu_s = 0$ case. A similar conclusion is reached when

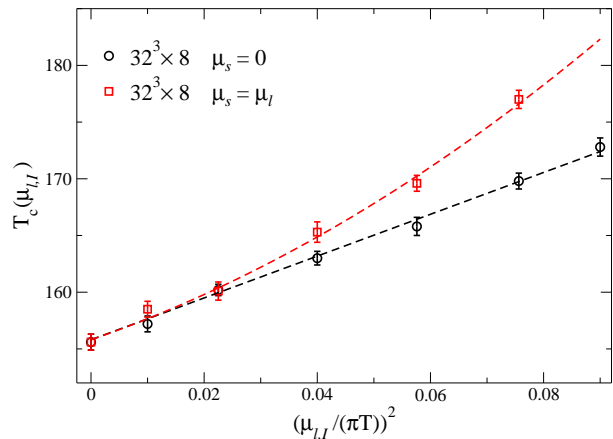


FIG. 7: Critical lines for the $32^3 \times 8$ lattices in the two different setups: $\mu_s = 0$ and $\mu_s = \mu_l$.

a common fit to both sets of data (i.e. with a common value for $T_c(0)$) is performed, as shown in the right panel of Fig. 8 and in Fig. 7.

We conclude that, for $\mu_s = 0$, no evidence of quartic corrections is found in the whole explored range. As a consequence, the extracted κ is stable against variations of the fitted range and we can exclude the presence of significant systematic corrections, related to the procedure of analytic continuation, affecting the continuum extrapolated determination of κ that we have provided.

In the case $\mu_s = \mu_l$, larger values of κ are obtained when quartic corrections are neglected, however κ becomes compatible with that obtained for $\mu_s = 0$ when such corrections are included, or when the fitted range of chemical potentials is small enough. We conclude that κ is not affected by the inclusion of μ_s , at least within present errors, which however are larger than for the $\mu_s = 0$ case. In particular, a fair estimate in this case is $\kappa(\mu_s = \mu_l) = 0.013(3)$.

IV. CONCLUSIONS

In the present study, we have extended results reported in Ref. [29] by performing numerical simulations on lattices with $N_t = 10, 12$ and aspect ratio 4, and by enlarging the range of chemical potentials explored for $N_t = 8$. That has permitted us to obtain continuum extrapolated results and to better estimate possible systematics related to analytic continuation.

Regarding the case $\mu_s = 0$, we have obtained continuum extrapolated values of κ from different observables (chiral susceptibility and the chiral condensate with two different renormalization prescriptions) and by two different extrapolation procedures (extrapolating κ_{cont} from $\kappa(N_t)$ or extracting κ_{cont} from continuum extrapolated temperatures). The comparison of the two different procedures permits us to give an estimate of the systematic uncertainties related to the continuum extrapolation.

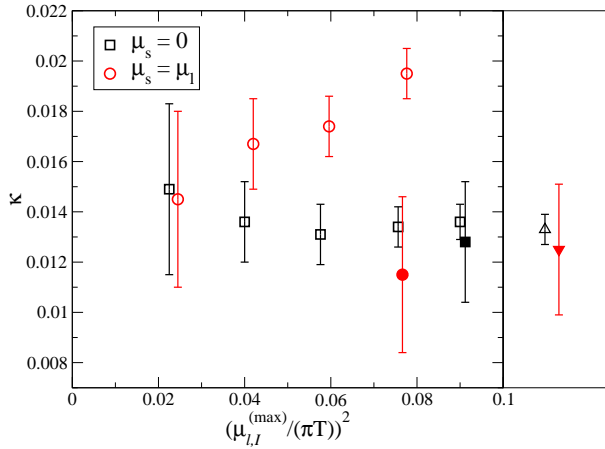


FIG. 8: Stability analysis of the fit to extract the κ value for the 32×8 lattice. Empty symbols correspond to purely quadratic fit while filled symbols also take into account the quartic correction; red circles represents the $\mu_s = \mu_l$ data, black squares the $\mu_s = 0$ ones. The right panel shows the result of a combined fit (i.e. fixing a common value for $T_c(0)$) to both data sets when a quartic correction is used for the $\mu_s = \mu_l$ data: the open (filled) triangle corresponds to $\mu_s = 0$ ($\mu_s = \mu_l$).

tion. In the case of the renormalized chiral susceptibility ($\kappa = 0.0132(10)$ vs $\kappa = 0.0131(12)$) the systematic error is negligible in comparison to the statistical one. In the case of $\langle \bar{\psi}\psi \rangle_{(1)}^r$ ($\kappa = 0.0134(13)$ vs $\kappa = 0.0145(11)$) and of $\langle \bar{\psi}\psi \rangle_{(2)}^r$ ($\kappa = 0.0127(14)$ vs $\kappa = 0.0138(10)$) the systematic and statistical uncertainties are clearly comparable in size. The extended analysis performed on $N_t = 8$ has permitted us to state also that, within present errors, systematic effects connected to the range of μ_l chosen to extract the curvature are not significant. Regarding finite size effects, the analysis reported in Ref. [29] already showed that they are negligible within the present precision on lattices with aspect ratio 4. Taking into account the obtained results and the contributions from the systematic effects mentioned above, we quote $\kappa = 0.0135(15)$ as our final continuum estimate for the case $\mu_s = 0$.

Such a result confirms, even after continuum extrapolation, a discrepancy with previous determinations obtained by Taylor expansion [15–17], reporting $\kappa \sim 0.006$. As already discussed quantitatively in Ref. [29], only part of this discrepancy can be accounted for by the different prescriptions used to determine the dependence of T_c on μ_l . Contrary to the Taylor expansion case, when working at imaginary μ_l one can use consistently the same prescription to locate T_c used for $\mu_l = 0$, i.e. looking for the maximum of the chiral susceptibility or the inflection point of the chiral condensate (see Ref. [29] for more details). The remaining part of the discrepancy could be possibly attributed to the systematic uncertainties related to the continuum extrapolation of previous studies. However, we stress that updated investigations

β	Lattice	$\chi_{\bar{\psi}\psi}$	$\langle \bar{\psi}\psi \rangle - 2(m_l/m_s)\langle \bar{s}s \rangle$	$\langle \bar{\psi}\psi \rangle/2$
3.50	32^4	1.97(4)	0.07999(11)	0.04403(5)
3.55	32^4	1.97(5)	0.05680(13)	0.03164(7)
3.60	32^4	2.05(6)	0.03912(14)	0.02211(7)
3.65	32^4	1.82(3)	0.02633(2)	0.01518(9)
3.70	32^4	1.80(3)	0.01804(3)	0.01064(2)
3.65	48^4	1.74(7)	0.02638(4)	0.01521(2)
3.75	48^4	1.61(5)	0.01232(5)	0.00749(2)
3.85	48^4	1.47(4)	0.00614(2)	0.00401(1)
3.95	48^4	1.37(3)	0.00331(2)	0.00237(1)

TABLE IV: Determination of the observables at $T = 0$ (on the 32^4 and 48^4 lattices) needed to perform the renormalizations discussed in Section II. Data are in lattice units.

by the same groups lead to results which are consistent with our estimate (see, e.g., Ref. [48]).

Regarding the case $\mu_s = \mu_l$, we have confirmed the preliminary results reported in Ref. [29]. There is evidence for the presence of quartic contributions in the dependence of T_c on the imaginary μ_B in this case and when such contributions are taken into account, or when the range of fitted chemical potentials around $\mu_B = 0$ is small enough, the curvature becomes compatible, even if within larger errors, with that obtained for $\mu_s = 0$. That means that also for the equilibrium conditions created in heavy ion collisions, corresponding to $\mu_s \sim 0.25 \mu_l$ around T_c , one does not expect significant deviations from the results obtained for $\mu_s = 0$: a prudential estimate for the curvature in this case is⁵ $\kappa = 0.0135(20)$. That is obtained based on the estimate for $\mu_s = 0$, with an increased error determined on the basis of the uncertainty that we have for the curvature extracted at $\mu_s = \mu_l$.

Finally, the analysis of the continuum extrapolated peak of the chiral susceptibility as a function of imaginary μ_B shows no significant variations of the strength of the transition, which could be associated to a possible nearby critical endpoint present along the pseudo-critical line.

Acknowledgments

FS received funding from the European Research Council under the European Community Seventh Framework Programme (FP7/2007-2013) ERC grant agreement No 279757. FN acknowledges financial support from the INFN SUMA project. Simulations have been performed on the BlueGene/Q Fermi at CINECA (Projects Iskra-B/EPDISIM, Iskra-B/CROWQCD and INF14.npqcd), and on the CSN4 Zefiro cluster of the Scientific Computing Center at INFN-PISA.

⁵ After completion of this work, Ref. [49] has appeared, reporting the consistent result $\kappa = 0.0149(21)$.

Appendix A: Data at $T = 0$

The determination of the renormalized condensate and susceptibility requires the computation of the corresponding quantities at $T = 0$ and at the same UV cutoff of the finite temperature data. To that aim, we spanned a range of β on the line of constant physics, $3.5 \leq \beta \leq 3.95$. The lattice sizes have been chosen in such a way to have temperatures well below T_c , keeping at the same time finite size effects under control. This required us to perform simulations on larger lattices (going from 32^4 up to 48^4) as we decreased the value of the lattice spacing. We report results in Table IV.

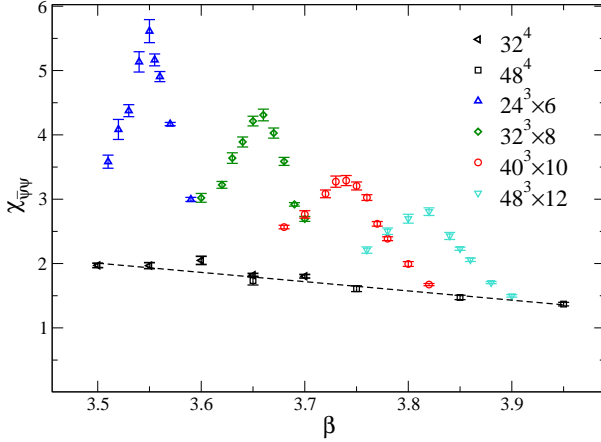


FIG. 9: Comparison between the $T = 0$ and $T \neq 0$ chiral susceptibility $\mu_B = 0$. The $T = 0$ susceptibility is needed to compute the renormalized chiral susceptibility, Eq. (13). Data are in lattice units and a linear fit to the $T = 0$ data is shown.

The temperatures, which are in the range $T \sim 25 - 50$ MeV, are low enough to be considered as a good approximation of the $T = 0$ limit; indeed, as expected because of the absence of transitions in this T range, observables depend smoothly on β ; moreover no dependence at all is expected on the imaginary chemical potentials, since they can be viewed as a modification in the temporal boundary conditions which, at $T = 0$ (i.e. for infinite temporal extension), are completely irrelevant. Hence, the relatively coarse sampling of the interval is enough to permit a reliable interpolation. We adopted a cubic spline interpolation for the condensate and a linear fit for the susceptibility.

The renormalization prescription for the susceptibility, Eq. (13), requires the subtraction of the $T = 0$ result from the finite T contribution. To give an idea of the relative magnitude of this subtraction, in Fig. 9 we plot $\chi_{\bar{\psi}\psi}$ for zero chemical potential and both at zero and finite T .

-
- [1] P. Braun-Munzinger, J. Stachel, J. P. Wessels and N. Xu, Phys. Lett. B **344**, 43 (1995) [nucl-th/9410026]; Phys. Lett. B **365**, 1 (1996) [nucl-th/9508020].
 - [2] F. Becattini, Z. Phys. C **69**, 485 (1996).
 - [3] F. Becattini and U. W. Heinz, Z. Phys. C **76**, 269 (1997) [Erratum-ibid. C **76**, 578 (1997)] [hep-ph/9702274].
 - [4] F. Becattini, J. Cleymans, A. Keranen, E. Suhonen and K. Redlich, Phys. Rev. C **64**, 024901 (2001) [hep-ph/0002267].
 - [5] P. Braun-Munzinger, D. Magestro, K. Redlich and J. Stachel, Phys. Lett. B **518**, 41 (2001) [hep-ph/0105229].
 - [6] A. Andronic, P. Braun-Munzinger and J. Stachel, Nucl. Phys. A **772**, 167 (2006) [nucl-th/0511071].
 - [7] J. Cleymans, H. Oeschler, K. Redlich and S. Wheaton, Phys. Rev. C **73**, 034905 (2006) [hep-ph/0511094].
 - [8] F. Becattini, M. Bleicher, T. Kollegger, T. Schuster, J. Steinheimer and R. Stock, Phys. Rev. Lett. **111**, 082302 (2013) [arXiv:1212.2431 [nucl-th]].
 - [9] Y. Aoki, G. Endrodi, Z. Fodor, S. D. Katz and K. K. Szabo, Nature **443** (2006) 675 [hep-lat/0611014].
 - [10] Y. Aoki, Z. Fodor, S. D. Katz and K. K. Szabo, Phys. Lett. B **643**, 46 (2006) [hep-lat/0609068].
 - [11] S. Borsanyi *et al.*, JHEP **1009**, 073 (2010).
 - [12] A. Bazavov, T. Bhattacharya, M. Cheng, C. DeTar, H. T. Ding, S. Gottlieb, R. Gupta and P. Hegde *et al.*, Phys. Rev. D **85**, 054503 (2012) [arXiv:1111.1710 [hep-lat]].
 - [13] T. Bhattacharya, M. I. Buchoff, N. H. Christ, H. - T. Ding, R. Gupta, C. Jung, F. Karsch and Z. Lin *et al.*, arXiv:1402.5175 [hep-lat].
 - [14] C. R. Allton, S. Ejiri, S. J. Hands, O. Kaczmarek, F. Karsch, E. Laermann, C. Schmidt and L. Scorzato, Phys. Rev. D **66**, 074507 (2002) [hep-lat/0204010].
 - [15] O. Kaczmarek, F. Karsch, E. Laermann, C. Miao, S. Mukherjee, P. Petreczky, C. Schmidt, W. Soeldner and W. Unger, Phys. Rev. D **83**, 014504 (2011) [arXiv:1011.3130 [hep-lat]].
 - [16] G. Endrodi, Z. Fodor, S. D. Katz and K. K. Szabo, JHEP **1104**, 001 (2011) [arXiv:1102.1356 [hep-lat]].
 - [17] S. Borsanyi, G. Endrodi, Z. Fodor, S. D. Katz, S. Krieg, C. Ratti and K. K. Szabo, JHEP **1208**, 053 (2012) [arXiv:1204.6710 [hep-lat]].
 - [18] P. de Forcrand and O. Philipsen, Nucl. Phys. B **642**, 290

- (2002) [hep-lat/0205016]; Nucl. Phys. B **673**, 170 (2003) [hep-lat/0307020].
- [19] M. D’Elia and M. P. Lombardo, Phys. Rev. D **67**, 014505 (2003) [hep-lat/0209146]; Phys. Rev. D **70**, 074509 (2004) [hep-lat/0406012].
- [20] V. Azcoiti, G. Di Carlo, A. Galante and V. Laliena, Nucl. Phys. B **723**, 77 (2005) [hep-lat/0503010].
- [21] L. K. Wu, X. Q. Luo and H. S. Chen, Phys. Rev. D **76**, 034505 (2007) [hep-lat/0611035].
- [22] P. Cea, L. Cosmai, M. D’Elia and A. Papa, Phys. Rev. D **77**, 051501 (2008) [arXiv:0712.3755 [hep-lat]].
- [23] P. Cea, L. Cosmai, M. D’Elia, C. Manneschi and A. Papa, Phys. Rev. D **80**, 034501 (2009) [arXiv:0905.1292 [hep-lat]].
- [24] P. Cea, L. Cosmai, M. D’Elia and A. Papa, Phys. Rev. D **81**, 094502 (2010) [arXiv:1004.0184 [hep-lat]].
- [25] K. Nagata and A. Nakamura, Phys. Rev. D **83**, 114507 (2011) [arXiv:1104.2142 [hep-lat]].
- [26] P. Cea, L. Cosmai, M. D’Elia, A. Papa and F. Sanfilippo, Phys. Rev. D **85**, 094512 (2012) [arXiv:1202.5700 [hep-lat]].
- [27] E. Laermann, F. Meyer and M. P. Lombardo, J. Phys. Conf. Ser. **432**, 012016 (2013). E. Laermann, F. Meyer and M. P. Lombardo, arXiv:1304.3247 [hep-lat].
- [28] P. Cea, L. Cosmai and A. Papa, Phys. Rev. D **89**, 074512 (2014) [arXiv:1403.0821 [hep-lat]].
- [29] C. Bonati, M. D’Elia, M. Mariti, M. Mesiti, F. Negro and F. Sanfilippo, Phys. Rev. D **90**, 114025 (2014) [arXiv:1410.5758 [hep-lat]].
- [30] Z. Fodor and S. D. Katz, JHEP **0203**, 014 (2002) [hep-lat/0106002].
- [31] Z. Fodor and S. D. Katz, JHEP **0404**, 050 (2004) [hep-lat/0402006].
- [32] S. Kratochvila and P. de Forcrand, PoS LAT **2005**, 167 (2006) [hep-lat/0509143].
- [33] A. Alexandru, M. Faber, I. Horvath and K. F. Liu, Phys. Rev. D **72**, 114513 (2005) [hep-lat/0507020].
- [34] P. Weisz, Nucl. Phys. B **212**, 1 (1983).
- [35] G. Curci, P. Menotti and G. Paffuti, Phys. Lett. B **130**, 205 (1983) [Erratum-ibid. B **135**, 516 (1984)].
- [36] C. Morningstar and M. J. Peardon, Phys. Rev. D **69**, 054501 (2004) [hep-lat/0311018].
- [37] A. Bazavov *et al.* [HotQCD Collaboration], PoS LAT-TICE **2010**, 169 (2010) [arXiv:1012.1257 [hep-lat]].
- [38] A. Bazavov, D. Toussaint, C. Bernard, J. Laiho, C. Detar, L. Levkova, M. B. Oktay and S. Gottlieb *et al.*, Rev. Mod. Phys. **82**, 1349 (2010) [arXiv:0903.3598 [hep-lat]].
- [39] Y. Aoki, S. Borsanyi, S. Durr, Z. Fodor, S. D. Katz, S. Krieg and K. K. Szabo, JHEP **0906**, 088 (2009) [arXiv:0903.4155 [hep-lat]].
- [40] S. Borsanyi, G. Endrodi, Z. Fodor, A. Jakovac, S. D. Katz, S. Krieg, C. Ratti and K. K. Szabo, JHEP **1011**, 077 (2010) [arXiv:1007.2580 [hep-lat]]; S. Borsanyi, Z. Fodor, C. Hoelbling, S. D. Katz, S. Krieg and K. K. Szabo, Phys. Lett. B **730**, 99 (2014) [arXiv:1309.5258 [hep-lat]].
- [41] A. Bazavov, H.-T. Ding, P. Hegde, O. Kaczmarek, F. Karsch, E. Laermann, Y. Maezawa and S. Mukherjee *et al.*, Phys. Rev. Lett. **113**, 072001 (2014) [arXiv:1404.6511 [hep-lat]].
- [42] S. Borsanyi, Z. Fodor, S. D. Katz, S. Krieg, C. Ratti and K. K. Szabo, Phys. Rev. Lett. **111**, 062005 (2013) [arXiv:1305.5161 [hep-lat]].
- [43] M. Cheng, N. H. Christ, S. Datta, J. van der Heide, C. Jung, F. Karsch, O. Kaczmarek and E. Laermann *et al.*, Phys. Rev. D **77**, 014511 (2008) [arXiv:0710.0354 [hep-lat]].
- [44] A. Roberge and N. Weiss, Nucl. Phys. B **275** (1986) 734.
- [45] M. A. Clark, A. D. Kennedy and Z. Sroczynski, Nucl. Phys. Proc. Suppl. **140**, 835 (2005) [hep-lat/0409133].
- [46] M. A. Clark and A. D. Kennedy, Phys. Rev. D **75**, 011502 (2007) [hep-lat/0610047].
- [47] M. A. Clark and A. D. Kennedy, Phys. Rev. Lett. **98**, 051601 (2007) [hep-lat/0608015].
- [48] P. Hedge, talk at Lattice 2015, to appear as PoS(LATTICE 2015)141.
- [49] R. Bellwied, S. Borsanyi, Z. Fodor, J. Günther, S. D. Katz, C. Ratti and K. K. Szabo, arXiv:1507.07510 [hep-lat].